High-yield monolayer graphene grids for near-atomic resolution cryoelectron microscopy

Yimo Han[a,1], Xiao Fan[a], Haozhe Wang[b], Fang Zhao[c], Christopher G. Tully[c], Jing Kong[b], Nan Yao[d], and Nieng Yan[a,1]

[a]Department of Molecular Biology, Princeton University, Princeton, NJ 08544; [b]Department of Electrical Engineering and Computer Science, Massachusetts Institute of Technology, Cambridge, MA 02139; [c]Department of Physics, Princeton University, Princeton, NJ 08544; and [d]PRISM Imaging and Analysis Center, Princeton University, Princeton, NJ 08544

Contributed by Nieng Yan, November 22, 2019 (sent for review November 1, 2019; reviewed by Jun Lou and Qing-Tao Shen)

Cryogenic electron microscopy (cryo-EM) has become one of the most powerful techniques to reveal the atomic structures and working mechanisms of biological macromolecules. New designs of the cryo-EM grids—aimed at preserving thin, uniform vitrified ice and improving protein adsorption—have been considered a promising approach to achieving higher resolution with the minimal amount of materials and data. Here, we describe a method for preparing graphene cryo-EM grids with up to 99% monolayer graphene coverage that allows for more than 70% grid squares for effective data acquisition with improved image quality and protein density. Using our graphene grids, we have achieved 2.6-Å resolution for streptavidin, with a molecular weight of 52 kDa, from 11,000 particles. Our graphene grids increase the density of examined soluble, membrane, and lipoproteins by at least 5-fold, affording the opportunity for structural investigation of challenging proteins which cannot be produced in large quantity. In addition, our method employs only simple tools that most structural biology laboratories can access. Moreover, this approach supports customized grid designs targeting specific proteins, owing to its broad compatibility with a variety of nanomaterials.

structure determination | cryo-EM | graphene grid | UV/ozone | high resolution

Cryogenic electron microscopy (cryo-EM) provides an effective way to investigate the structures of biological macromolecules (1–4). Technological breakthroughs in direct electron detection (5, 6) and advanced algorithms (6–8) have enabled cryo-EM to map the precise structural details of biological macromolecules at near-atomic resolutions (9), which is essential for the understanding of their functions. As the cryo-EM community expands, a shared view of many researchers is that the bottleneck for cryo-EM resides in sample preparation. Cryo-EM requires protein particles to be suspended in a thin layer of vitrified ice to avoid denaturation (10, 11). To achieve this, continuous amorphous carbon films and holey carbon grids (Quantifoil) have been widely used. Following glow-discharge plasma treatment, these grids become hydrophilic and allow the formation of a thin layer of aqueous solution upon blotting by a filter paper (12).

Among these grids, the continuous carbon film (usually 20 nm thick) inevitably introduces electron scattering that adds noise and reduced image resolution. Therefore, holey carbon grids, where the layer of solution can form in the hole area, have been considered the preferred cryo-EM grids for high-resolution single-particle analysis. However, due to the distinct protein properties, for which we coined a term "proteinality," Quantifoil grids do not work for all proteins. While some proteins prefer to attach to the carbon film and fail to enter the holes, others stay on the air–water interface with compromised folding (13). In addition, the nonuniformity of ice thickness makes it difficult to search across the entire grids for thin ice areas, where the image contrast is optimal for high-resolution image processing. Since thin ice and high protein density are key to high-resolution reconstruction of the protein structure, a better design of the cryo-EM grid that can solve these problems will benefit the cryo-EM community.

Graphene materials (such as graphene oxide [GO]) (14) have been used as supporting films in cryo-EM to improve the protein density in the hole areas of Quantifoil grids (15–18) (schematically shown in Fig. 1 *A* and *D*). Compared to films made by other materials, graphene derivatives have the advantages of being intrinsically thin and made of only light elements (carbon, oxygen, hydrogen, etc). These advantages make functional graphene transparent to 300-kV electrons. Among the graphene materials, GO films have been tested using 20S proteasome (700 kDa) at a low concentration (tens of micrograms per milliliter) to reconstruct a structure at ∼2.5-Å resolution with reasonable adsorption (19). Despite the improvements of protein adsorption, these grids have yet to be widely used in the community mainly for 3 reasons: 1) low coverage of graphene limits the effective areas to acquire cryo-EM data; 2) nonuniform surface contamination results in either protein aggregation or no adsorption; and 3) an intricate fabrication process or requirement of expensive instruments that most structural biology laboratories have little access to.

Here, we demonstrate a more convenient and less costly approach to fabricating high-quality graphene cryo-EM grids with nearly full graphene coverage (Fig. 1*B*) and clean graphene surfaces (Fig. 1*C*), which provide a uniform and thin ice layer

Significance

Single-particle cryogenic electron microscopy (cryo-EM) represents the cutting-edge technology for structural determination of biomacromolecules. However, technical challenges associated with cryosample preparation limit cryo-EM from achieving higher resolution for broader range of targets. Here, we demonstrated a high-yield, monolayer graphene-supporting film improved the cryosample quality. Using this approach, we have achieved, so far, the highest resolution structure of the smallest protein by cryo-EM with the minimal number of datasets. Our technique paves the way for more general cryosample preparation for near-atomic resolution cryo-EM.

Author contributions: Y.H. and N. Yan designed research; Y.H. and X.F. performed research; Y.H., H.W., and J.K. contributed new reagents/analytic tools; Y.H., X.F., F.Z., C.G.T., and N. Yao analyzed data; and Y.H. and X.F. wrote the paper.

Reviewers: J.L., Rice University; and Q.S., ShanghaiTech University.

Competing interest statement: The authors N. Yan and Y.H. are inventors on the patent application entitled "Fabrication of nanomaterial cryogenic electron microscopy (cryo-EM) grids."

Data deposition: The data reported in this paper have been deposited in the Electron Microscopy Data Bank (EMDB) (accession no. EMD-20907) and Electron Microscopy Public Image Archive (EMPIAR) (accession no. EMPIAR-10335).

[1]To whom correspondence may be addressed. Email: yimoh@princeton.edu or nyan@princeton.edu.

This article contains supporting information online at https://www.pnas.org/lookup/suppl/doi:10.1073/pnas.1919114117/-/DCSupplemental.

First published December 26, 2019.

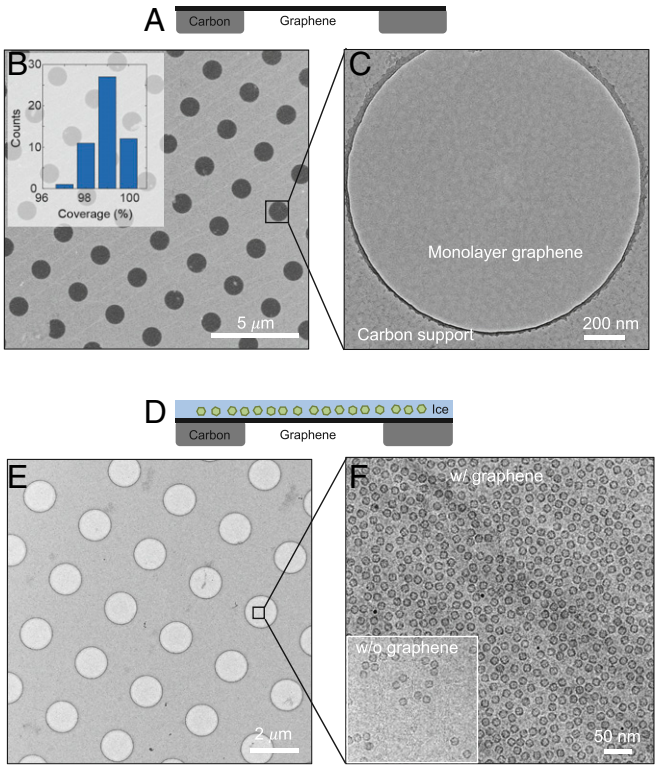

Fig. 1. High-yield graphene grids for cryo-EM. (*A*) Side-view schematic of graphene grids. (*B*) Large-scale SEM image of graphene film on holey carbon Quantifoil grids. All of the holes in this area are covered by suspended graphene. The *Inset* displays the statistics of graphene yield. On average, 99% of graphene has been successfully suspended over holes. The statistics were conducted by counting the yield of suspended graphene in 50 squares. More statistics from different batches are shown in *SI Appendix*, Fig. S1. (*C*) Zoomed-in TEM image of suspended graphene, showing its uniformity and cleanness. (*D*) Side-view schematic of cryo-EM sample on graphene grids. (*E*) Low-magnification image of a cryo-EM sample using graphene grids. The uniformity and cleanness of graphene contributes to a uniform and thin ice layer with embedded proteins. (*F*) Cryo-EM micrograph of apoferritin on graphene grids, compared to the same sample on holey carbon grids (*Inset*). The apoferritin concentration in solution is 1.2 mg/mL.

(Fig. 1*E*) and improve the protein density (Fig. 1*F*) for single-particle cryo-EM analysis.

Results

Fabrication of Graphene Grids. We fabricated graphene cryo-EM grids by transferring continuous monolayer graphene from its original substrate, a copper foil, to a Quantifoil holey carbon grid using an organic molecule-assisted transfer method, as schematically described in Fig. 2*A* (more details in *SI Appendix*, Fig. S2). With a thin layer of methyl methacrylate (MMA) to support graphene during the transfer process, our method results in a very high percentage coverage of hole areas by suspended graphene. Fig. 1*B* shows a scanning electron microscopy (SEM) image of a graphene grid where all holes in the holey carbon film are covered without any broken ones. Statistics from different areas indicate that the average yield of suspended monolayer graphene is ~99% (Fig. 1 *B*, *Inset*), higher than any previously reported functional graphene cryo-EM grids. The high yield of graphene using this method is consistent from batch to batch (*SI Appendix*, Fig. S1). In addition, our cleaning process is sufficient to remove most organic molecule residues and achieve a clean graphene surface (Fig. 1*C*). The entire fabrication process takes about a few hours, and the production of up to hundreds of grids can be done en masse without the special requirement of equipment or large quantity of reagent (an overview of the method appears in *SI Appendix*, Fig. S2 and a video demonstration in Movie S1).

Since graphene is hydrophobic, its natural surfaces show limited adsorption of proteins (*SI Appendix*, Fig. S3). Conventional glow-discharge plasma cleaning (Ar or O_2 plasma) that has been widely used to generate hydrophilic carbon films will damage graphene within seconds, owing to the atomic thinness of graphene. Instead, we employed UV/ozone, which uses ultraviolet (UV) irradiation to generate a small amount of ozone gas to gently oxidize sample surfaces (Fig. 2*B*). UV/ozone has been widely used to clean the surface of semiconductors and polymers (20, 21). The ozonation of monolayer graphene forms oxygenated functional groups, which can effectively render the surface of graphene hydrophilic (22–24).

UV/ozone has the advantage of adding functional groups to graphitic surfaces at a slow, and thus, controllable rate, therefore, fine tuning the surface properties of graphene. The contact-angle measurements (Fig. 2*C*) demonstrate that graphene gradually becomes hydrophilic as the UV exposure time increases. Within 10 min, UV/ozone effectively converts graphene into a hydrophilic graphene derivative, as shown in the orange box in Fig. 2*C*. Raman spectroscopy (Fig. 2*D*) indicates that the hydrophilic graphene derivative after 10 min of UV irradiation is composed of oxygenated graphene (orange curve in Fig. 2*D*), while 5 more minutes of UV irradiation turns graphene into complete GO (blue curve in Fig. 2*D*). X-ray photoelectron spectroscopy (XPS) analysis (*SI Appendix*, Fig. S4*A*) indicates an increment of carboxylic groups and C–O bonds from the oxygenated functional groups. In the XPS plots, a noticeable drop of C–O peak appears in the sample in UV irradiation after 10 min, indicating that a cleaning process removes the surface contaminants on graphene due to air exposure. In addition, we found that under UV irradiation, graphene films can survive up to an hour, where nanopores start to emerge and expand (*SI Appendix*, Fig. S4*B*). As the 10-min treatment is relatively gentle and presents clean and uniform surfaces with good hydrophilicity, we used this parameter to treat our graphene for the following cryo-EM experiments.

A 2.2-Å Resolution Reconstruction of Apoferritin with Graphene Grids. To demonstrate that our high-quality graphene grids are suitable and practical for cryo-EM at near-atomic resolution, we prepared standard apoferritin on our graphene grids for cryo-EM data collection and single-particle analysis (Fig. 1*F*). In addition to the improved protein density, we have reached a high-resolution reconstruction of apoferritin at 2.2 Å (Fig. 3*A* and *SI Appendix*, Fig. S5*A*). The resolution was determined by gold standard Fourier shell correlation (FSC) (*SI Appendix*, Fig. S5*B*), where the information limit has already reached the Nyquist frequency of the input micrographs, indicating our graphene grids are suitable for resolution beyond 2.2 Å. In the reconstructed local density maps, we were able to clearly dock individual residues in the side chain from the published Protein Data Bank (PDB) model (Fig. 3*B*). In addition, the central holes of the benzene rings were clearly resolved in the density map (Fig. 3*B*, Phe_{51} and Tyr_{137}), confirming we have achieved a veritable high resolution using the graphene grids. Our reconstruction of apoferritin at 2.2-Å resolution is the highest among those in the EM Data Bank (EMDB) using GO or other thin film-supported grids. These results indicate the bountiful potential of our graphene grids in cryo-EM investigations of protein structures at a near-atomic resolution.

A 2.6-Å Resolution Reconstruction of 52 kDa Streptavidin with Graphene Grids. The advantages of using graphene cryo-EM grids can be divided into 2 categories. For small proteins (<200 kDa), graphene-supporting film can effectively reduce the ice thickness without

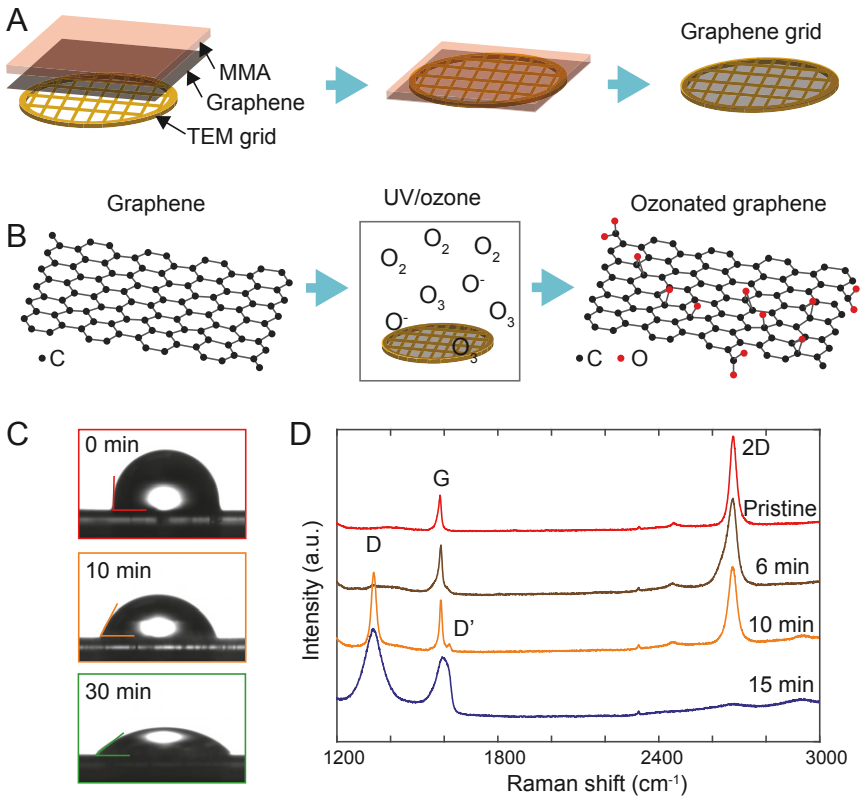

Fig. 2. Fabrication of graphene cryo-EM grids. (*A*) Schematic summary of graphene grid fabrication process. More details are provided in *SI Appendix*, Fig. S2. (*B*) Schematic of surface treatment by UV irradiation. The ozonation of graphene adds oxygenated functional groups to the graphene surface, which makes the graphene derivative hydrophilic. (*C*) Contact angle measurements showing that UV/ozone treatment increases the hydrophilicity (original graphene: 89.4°; 10 min: 71.6°; 30 min: 45.5°). (*D*) Raman spectroscopy shows that 10-min UV/ozone treatment can convert graphene (indicated by the G peak) to oxygenated graphene by creating disorders (indicated by the D and D′ peaks in the orange curve). Fifteen minutes of UV/ozone can effectively convert graphene into GO (blue curve).

introducing background noise to the images, allowing for higher resolution structural determination of the proteins. For membrane proteins embedded in detergent micelles or liposomes, which are usually hard to acquire in large quantities, graphene grids can improve the protein adsorption, thus overcoming the issues of low protein concentration. Therefore, we evaluated the practical behavior of our graphene grids using a 52-kDa small soluble protein and a membrane protein in detergent micelles and liposomes.

We deposited 52 kDa streptavidin (the smallest soluble protein that has been solved hitherto in EMDB) onto freshly UV/ozone-treated graphene grids to prepare frozen-hydrated streptavidin samples in Vitrobot with a general plunge freezing method. The overall grid montage collected in cryo-EM displays more than 70% of the grid squares containing thin ice layers that are suitable for data collection (*SI Appendix*, Fig. S6 *A* and *B*). Each grid square possesses a uniform thin ice layer with proteins embedded in it (*SI Appendix*, Fig. S6 *C* and *D*), where it is not necessary to screen for good areas in high magnification to save time and effort. After data acquisition, the 52 kDa streptavidin particles could be identified clearly from the motion-corrected micrographs (Fig. 4*A*). The good image contrast under such a small defocus value of −0.85 μm further confirms that the ice is much thinner than that in cryosamples using conventional grids. Furthermore, the first-order reciprocal lattice of graphene could be identified precisely in the Fourier transform of the micrograph (Fig. 4*B*). The sharp peaks (circled in orange in Fig. 4*B*) indicate that the raw information contained in the micrograph could reach to at least 2.14 Å in frequency.

After single-particle analysis using Relion (25) (details in *SI Appendix*, Fig. S7), we obtained the structure of apostate streptavidin at 2.6-Å resolution (Fig. 4*C*), where the density map has demonstrated convincing structural information of the residues in the beta strands (Fig. 4*D*). The structure resolution was estimated from gold standard FSC criteria (Fig. 4*E*) and the quality of the reconstruction was further validated by local resolution and directional 3-dimensional (3D)-FSC analysis (*SI Appendix*, Fig. S8 *A*–*D*). In addition, the final reconstruction of the 2.6-Å structure was obtained from only ∼11,000 streptavidin particles with an estimated Rosenthal–Henderson B factor of 72.8 Å^2 (*SI Appendix*, Fig. S8*E*). This is much smaller than previously published reconstruction results of streptavidin (26), indicating that

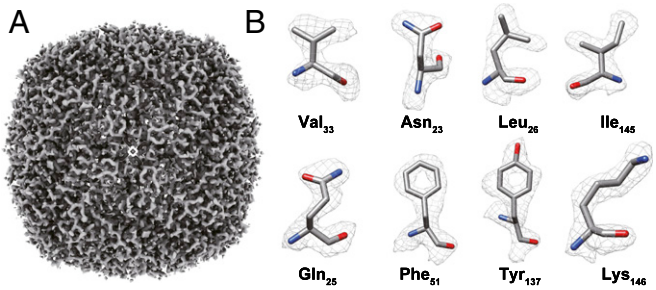

Fig. 3. Graphene grids for standard apoferritin. (*A*) Single-particle reconstruction of apoferritin at 2.2-Å resolution. (*B*) Representative density maps of selected residues (fitted with PDB model 1FHA, ref. 37) demonstrate convincing side chain structures.

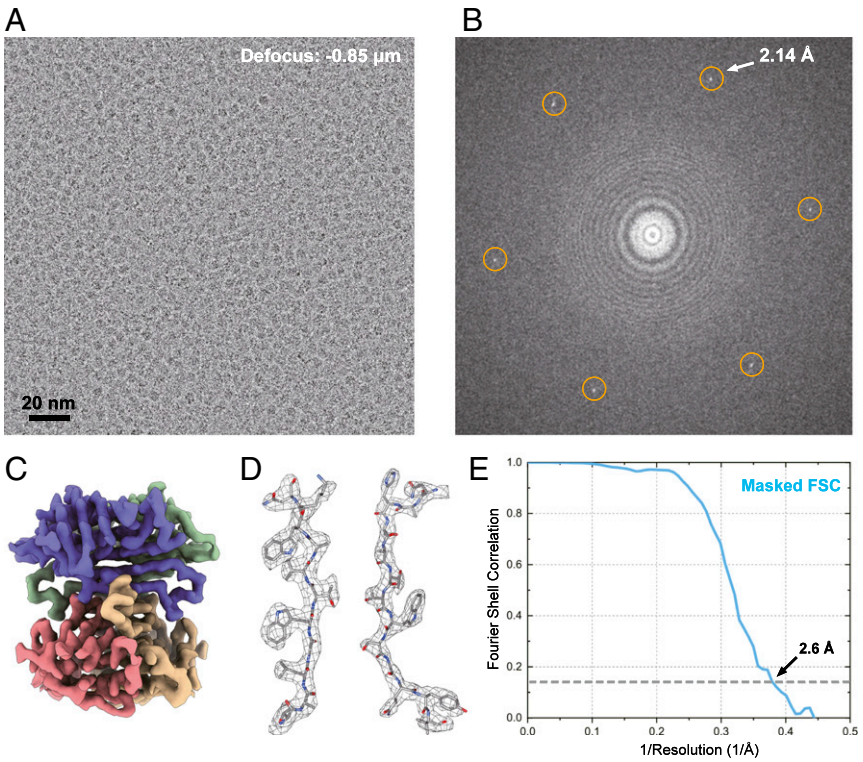

Fig. 4. Graphene grids for small soluble proteins. (*A*) Cryo-EM micrograph of 52 kDa streptavidin particles. Despite a small defocus value (−0.85 μm), streptavidin proteins present nice contrasts in the micrograph. (*B*) Fourier transform of *A* with graphene reciprocal lattice circled in orange. (*C*) Single-particle reconstruction of 52 kDa streptavidin at 2.6-Å resolution. (*D*) Representative density maps of 2 beta strands (fitted with PDB model 6J6K, ref. 38). (*E*) Gold standard FSC (criteria 0.143) curve of the masked map with a reported resolution of 2.6 Å.

the high-resolution information is better preserved using our graphene grids.

High Density of Membrane and Lipoproteins on Graphene Grids. Unlike most soluble proteins, membrane proteins are usually more difficult to obtain in large quantity or high protein concentration. Testing with a bacteria sodium channel (NaChBac) purified in detergent micelles, we observed a 5-fold improvement of the protein density using our graphene grids (Fig. 5*A* vs. Fig. 5*B*). Despite the adsorption of the membrane proteins on graphene-supporting film, we observed a reasonable distribution of different views, which is essential for further single-particle data processing. In addition, we reconstitute NaChBac into liposomes for structural investigation, which can provide more orientations of the protein for single-particle analysis, as well as reproducing more of the proteins' native physiological environments. The long-time historical challenge to investigate the structure of lipoproteins is the low density of liposomes on a cryo-EM holey carbon grids (27, 28) (Fig. 5*C*). However, our graphene grids remarkably improve the liposome density by providing a hydrophilic surface to attract liposomes (Fig. 5*D*). These results imply that our graphene grids can assist single-particle cryo-EM on membrane proteins in detergent micelles (or potentially lipid nanodiscs), as well as liposomes by improving the protein density. Our grids will reduce the requirements of cryo-EM sample preparation, allowing for structural investigation of membrane proteins that cannot be produced in large quantity or concentrated to high concentration.

Conclusions and Discussions

In summary, we developed a robust approach to produce high-quality graphene grids for cryo-EM with about 99% suspended graphene coverage. Our graphene grids provide thinner ice layers and an increased protein density. We have achieved a 2.6-Å resolution structure of 52 kDa streptavidin and a 2.2-Å resolution structure of standard apoferritin. For membrane proteins and lipoproteins that are usually hard to prepare in large quantities, we have achieved more than 5-fold improvement of protein density, which will aid the studies of membrane proteins in their more native environments. In addition, the method we described to make graphene grids can be easily accessed by most structural biology research groups with reasonable expense. Our method can also be applied to other nanomaterials such as 1-dimensional nanowires and nanotubes, which can allow for more sophisticated grid design targeting specific proteins. We expect our method to benefit the cryo-EM community by improving the sample preparation process.

Materials and Methods

Continuous Monolayer Graphene Synthesis. In this research, commercial copper foils with 99.8% purity (Alfa Aesar no. 13382) were used as the substrate to grow single-layer graphene by chemical vapor deposition (CVD) method. Before growth, we used nickel etchant (Nickel Etchant TFB by Transene Company, Inc.) to clean the surface of the copper foil. The foil was then placed in a CVD system with a base pressure of 35 mTorr. The foil was annealed in the CVD chamber for 30 min at 1,030 °C with a 10 standard cubic centimeter per minute (sccm) H_2 flow. Subsequently, single-layer graphene was grown at the same temperature (1,030 °C) with 60 sccm H_2 and 3.5 sccm CH_4 for 30 min to form a continuous monolayer. The graphene growth protocol is similar to the one used in ref. 29. Alternatively, continuous monolayer graphene on copper foil can be purchased from Graphene Supermarket.

Graphene Grid Fabrication. The graphene grown by CVD or alternatively purchased from Graphene Supermarket came with graphene on a copper foil on both sides. We first coated the graphene on copper foil with MMA EL 6 using a home-made spin coater at the speed of ~2,500 rpm for 1 min (Movie S1). The MMA/graphene/Cu/backside graphene can be kept at room

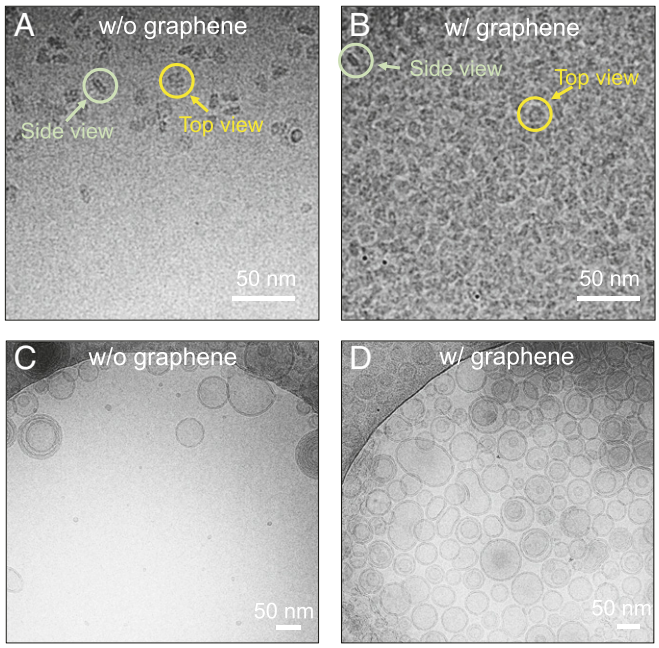

Fig. 5. Graphene grids for membrane protein and liposomes. (*A*) Cryo-EM micrograph of a bacterial sodium channel (NaChBac) on holey carbon grids. (*B*) Cryo-EM micrograph of NaChBac on graphene grids, which increase the protein density by 5-fold. (The protein concentration in solution is 6 mg/mL.) (*C*) Cryo-EM micrograph of liposomes on holey carbon grids, where the liposomes prefer to adsorb to the amorphous carbon-supporting film. (*D*) Cryo-EM micrograph of liposomes on graphene grids. The liposomes adsorbed to the graphene surface uniformly, allowing for cryo-EM data acquisition in the thin ice on graphene over the hole areas.

temperature in air for a few months without severer copper oxidation. After coating the sample with a thin layer of MMA, the sample was placed in a glow-discharge system backside up to remove the graphene grown on the backside of the copper foil (we used a typical glow-discharge condition: 30 s O_2 or Ar plasma).

Afterward, we used 1 M ammonium persulfate (APS) to etch the copper substrate by floating the MMA/graphene/Cu on APS with the MMA side facing up. Since it is hard to tell the backside from the topside, keeping track of the sides from the very beginning is highly encouraged. After the copper foils were entirely gone, we transferred the film (graphene with MMA) to deionized (DI) water twice, each for a 10-min interval (or you can transfer to DI water once and wait for more than 20 min). After that, we used the Quantifoil (Au 1.2/1.3 300 mesh) to scoop out the MMA/graphene film and air dry. We noted that the Quantifoil Au 1.2/1.3 300 mesh grids have a large variation of hole sizes (from ∼500 nm to 1.3 μm). Our method works for most within this range. A slightly lower yield was observed for Quantifoil grids with 2-μm hole size. Alternatively, the polymer state of MMA, poly methyl methacrylate (PMMA), can also be used to make graphene cryo-EM grids. PMMA has been commonly used in materials science for transferring nano structures (30, 31), but the high molecular weight of PMMA results in more polymer residues after the transfer process.

Afterward, we placed the grid on a hot plate and baked at ∼130 °C for ∼20 min, which assists the graphene in stitching to the Quantifoil carbon. Otherwise, the graphene film will detach from the grid in the cleaning process. Then we picked up the grid and waited for it to cool down, followed by soaking the grids into acetone vertically. We placed the grids in warm acetone for 30 min to dissolve the MMA. Then we transferred the grids to another fresh acetone to further clean the MMA. Afterward, we transferred all grids to isopropyl alcohol (IPA) to clean off the acetone residue. The process to transfer grids from one organic solvent to another should be very fast to avoid the acetone drying in any case. We took the grid out of IPA vertically and used a filter paper to draw remaining IPA away from the grids. Then, we left the grids on a filter paper to air dry them. Afterward, we placed the grids on a hot plate for another ∼20 min to bake off organic residues. This baking process is for removing the IPA residues. The graphene grids were then checked in a transmission electron microscope (TEM) or an SEM to confirm the yield and cleanness. The process described above can result in a high yield of suspended, clean graphene films on Quantifoil holey carbon grids. Repeating the acetone-IPA baking process can further clean graphene surfaces. More details can be found in Movie S1. This method was adapted from previous work (32, 33). The materials used in the transfer process are as follows: Graphene on Cu was purchased from Graphene Supermarket; MMA EL 6 (item no. M310006 0500L1GL) and PMMA 495 A4 (item no. M130004 0500L1GL) were purchased from MicroChem (now Kayaku); the spin coater was made from a computer fan (Movie S1); APS was purchased from Sigma-Aldrich; and Quantifoil TEM grids were purchased from EMS.

UV/Ozone. We used an UV/ozone cleaner (UVOCS T10 × 10 system) to treat graphene surfaces and make graphene grids hydrophilic. This tool is commonly used for cleaning of wafers contaminated with organic substrates. The UV/ozone used a low pressure, quartz, mercury vapor lamp to generate 185 nm and 254 nm of UV light. The process took place at room temperature for 10 min. A temperature rise was observed upon prolonged cleaning. The surface-treated graphene grids were used for cryosample preparation on the same day. An exposure of the surface-treated graphene grids to the air for more than a day may introduce surface contamination or broken graphene that reduces the yield.

Characterization of Graphene Grids. The samples for contact angle measurements are prepared following exactly the same process as for graphene grids but using optical cover slits as the substrate materials instead of Quantifoil grids. We employed a contact-angle goniometer (Rame–Hart goniometry) to measure the contact angle of a 2-mL drop of DI water on the graphene surface. Immediately after applying the droplet, the contact angle was measured by taking the average of a series of 5 small time intervals on each side (left and right).

The graphene sheets on glass slides after different UV/ozone treatments were characterized by Raman spectroscopy on a Horiba Jobin-Yvon LabRAM aramis Raman system using a 100× objective lens with a numerical aperture (NA) of 0.95. The excitation source for Raman spectroscopy is a 532 nm laser (2.33 eV) with a laser power 0.6 mW to avoid laser-induced heating. The acquisition time is 10 s with 5 accumulations.

High-resolution (HR) XPS analysis of graphene samples was conducted using a Thermo Fisher K-Alpha X-ray Photoelectron Spectrometer. The system is equipped with a monochromatic X-ray source and a focusing lens allowing for analysis area from 30 to 400 μm in 5-μm steps. In this study, we selected a 400-μm X-ray spot for all XPS measurements. Survey spectra were taken at 200 eV pass energy and the HR spectra for carbon ground state electron configuration 1s subshell (C1s) region was recorded at 20 eV pass energy. The XPS system has been calibrated by recording a clean Au sample with the Au 4f7/2 binding energy at 84.0 eV. Chemical compositions were determined using CasaXPS (Casa Software Ltd.)-fitting software.

Streptavidin Cryo-EM Sample Preparation. Streptavidin stock solution (1 mg/mL, New England Biolabs, N7021s) was diluted to 0.5 mg/mL using DI water. UV/ozone freshly treated graphene grids (Quantifoil 300 mesh Au R1.2/1.3) were used to prepare cryosamples. In Vitrobot Mark IV (Thermo Fisher), 4 μL of 0.5 mg/mL sample was applied to the grid for 30 s before blotting. The blot time was 4 s with a blot force of 0 in the Vitrobot. After blotting, the grid was rapidly plunged into liquid ethane for the vitrification.

Data Collection. A total number of 1,086 raw movie stacks were automatically collected in 12 h by SerialEM 3.7 on a 300 kV Cs-corrected Titan Krios using a K2 Summit detector (with GIF Bio-Quantum Energy Filters, Gatan). We collected the raw movies in K2 counted mode at a magnification of 215,000 (in energy-filtered TEM [EFTEM] mode, spot size 6, C2 aperture 70 μm) with a pixel size of 0.536 Å. The total exposure time was set to 2.4 s with a 0.075-s frame time to generate 32-frame gain normalized stacks in MRC format. The total dose for a stack is 49 $e^-/Å^2$.

Data Processing. Movie stacks were motion corrected using Relion's interpretation with a 5 × 5 patch and a 2-fold binning. Full-frame contrast transfer function (CTF) values were estimated from nondose weighted images by CTFFind4.1 (34) in Relion with exhaustive searching. Particles were automatically picked with the Laplacian-of-Gaussian method in Relion autopicking. After the particle extraction, the particle stacks were given a 120-Å high pass filter (using relion_image_handler–highpass 120) for the following processes: Multiple rounds of 2D classification, 3D classification, 3D autorefine. CTF refinement and Bayesian polishing were performed in Relion 3.0 with standard procedure (7), where the CTF corrections were

performed during 3D autorefine. Density maps were prepared by University of California San Francisco Chimera (35) and Chimera X (36).

Data Availability. Data supporting the findings of this manuscript are available in public repositories. The accession no. for the EM map of streptavidin reported in this paper is EMD-20907. The raw data were deposited at EMPIAR-10335.

ACKNOWLEDGMENTS. The work is supported by the Dean for Research Innovation Fund for New Ideas in the Natural Sciences from Princeton University. N. Yan is supported by the Shirley M. Tilghman endowed professorship from Princeton University. We acknowledge the use of Princeton's Imaging and Analysis Center, which is partially supported by the Princeton Center for Complex Materials, a National Science Foundation Materials Research Science and Engineering Centers (NSF-MRSEC) program (DMR-1420541). J.K. and H.W. acknowledge the support from the Center for Energy Efficient Electronics Science through NSF Grant 0939514. C.G.T. and F.Z. are supported by The Simons Foundation (377485) and John Templeton Foundation (58851). We thank Mengnan Zhao, Xuelan Wu, Hannah A. Ledford, Nguyen On, Ang-Yu Lu, Kibum Kang, Yunfan Guo, Hongwu Qian, Shuai Gao, Xin Zhao, Miaohui Hu, and Shiming Lei for helpful discussions.

1. N. Grigorieff, S. C. Harrison, Near-atomic resolution reconstructions of icosahedral viruses from electron cryo-microscopy. *Curr. Opin. Struct. Biol.* **21**, 265–273 (2011).
2. M. Liao, E. Cao, D. Julius, Y. Cheng, Structure of the TRPV1 ion channel determined by electron cryo-microscopy. *Nature* **504**, 107–112 (2013).
3. W. Kühlbrandt, Biochemistry. The resolution revolution. *Science* **343**, 1443–1444 (2014).
4. E. Nogales, S. H. W. Scheres, Cryo-EM: A unique tool for the visualization of macromolecular complexity. *Mol. Cell* **58**, 677–689 (2015).
5. A. R. Faruqi, R. Henderson, Electronic detectors for electron microscopy. *Curr. Opin. Struct. Biol.* **17**, 549–555 (2007).
6. X. Li *et al*., Electron counting and beam-induced motion correction enable near-atomic-resolution single-particle cryo-EM. *Nat. Methods* **10**, 584–590 (2013).
7. J. Zivanov *et al*., New tools for automated high-resolution cryo-EM structure determination in RELION-3. *eLife* **7**, e42166 (2018).
8. G. Tang *et al*., EMAN2: An extensible image processing suite for electron microscopy. *J. Struct. Biol.* **157**, 38–46 (2007).
9. Y. Cheng, Single-particle cryo-EM at crystallographic resolution. *Cell* **161**, 450–457 (2015).
10. J. Dubochet, J. J. Chang, R. Freeman, J. Lepault, A. W. McDowall, Frozen aqueous suspensions. *Ultramicroscopy* **10**, 55–61 (1982).
11. J. Dubochet, Cryo-EM–The first thirty years. *J. Microsc.* **245**, 221–224 (2012).
12. R. A. Grassucci, D. J. Taylor, J. Frank, Preparation of macromolecular complexes for cryo-electron microscopy. *Nat. Protoc.* **2**, 3239–3246 (2007).
13. I. Drulyte *et al*., Approaches to altering particle distributions in cryo-electron microscopy sample preparation. *Acta Crystallogr. D Struct. Biol.* **74**, 560–571 (2018).
14. D. R. Dreyer, S. Park, C. W. Bielawski, R. S. Ruoff, The chemistry of graphene oxide. *Chem. Soc. Rev.* **39**, 228–240 (2010).
15. R. S. Pantelic, J. C. Meyer, U. Kaiser, W. Baumeister, J. M. Plitzko, Graphene oxide: A substrate for optimizing preparations of frozen-hydrated samples. *J. Struct. Biol.* **170**, 152–156 (2010).
16. C. J. Russo, L. A. Passmore, Controlling protein adsorption on graphene for cryo-EM using low-energy hydrogen plasmas. *Nat. Methods* **11**, 649–652 (2014).
17. K. Naydenova, M. J. Peet, C. J. Russo, Multifunctional graphene supports for electron cryomicroscopy. *Proc. Natl. Acad. Sci. U.S.A.* **116**, 11718–11724 (2019).
18. N. Liu *et al*., Bioactive functionalized monolayer graphene for high-resolution cryo-electron microscopy. *J. Am. Chem. Soc.* **141**, 4016–4025 (2019).
19. E. Palovcak *et al*., A simple and robust procedure for preparing graphene-oxide cryo-EM grids. *J. Struct. Biol.* **204**, 80–84 (2018).
20. L. Zafonte, R. Chiu, *UV/Ozone Cleaning for Organics Removal on Silicon Wafers*, H. L. Stover, Ed. (International Society for Optics and Photonics, 1984), vol. 0470, pp. 164–177.
21. J. A. Poulis, J. C. Cool, E. H. P. Logtenberg, UV/ozone cleaning, a convenient alternative for high quality bonding preparation. *Int. J. Adhes. Adhes.* **13**, 89–96 (1993).
22. L. Cai, J. L. Bahr, Y. Yao, J. M. Tour, Ozonation of single-walled carbon nanotubes and their assemblies on rigid self-assembled monolayers. *Chem. Mater.* **14**, 4235–4241 (2002).
23. E. Najafi, J.-Y. Kim, S.-H. Han, K. Shin, UV-ozone treatment of multi-walled carbon nanotubes for enhanced organic solvent dispersion. *Colloids Surf. A Physicochem. Eng. Asp.* **284**, 373–378 (2006).
24. Z. Xu *et al*., Reversible hydrophobic to hydrophilic transition in graphene via water splitting induced by UV irradiation. *Sci. Rep.* **4**, 6450 (2014).
25. S. H. W. Scheres, A Bayesian view on cryo-EM structure determination. *J. Mol. Biol.* **415**, 406–418 (2012).
26. X. Fan *et al*., Single particle cryo-EM reconstruction of 52 kDa streptavidin at 3.2 Angstrom resolution. *Nat. Commun.* **10**, 2386 (2019).
27. L. Wang, F. J. Sigworth, Structure of the BK potassium channel in a lipid membrane from electron cryomicroscopy. *Nature* **461**, 292–295 (2009).
28. L. Tonggu, L. Wang, Cryo-EM sample preparation method for extremely low concentration liposomes. bioRxiv:10.1101/494997 (13, December 2018).
29. H. Wang *et al*., Low-temperature copper bonding strategy with graphene interlayer. *ACS Nano* **12**, 2395–2402 (2018).
30. L. Jiao *et al*., Creation of nanostructures with poly(methyl methacrylate)-mediated nanotransfer printing. *J. Am. Chem. Soc.* **130**, 12612–12613 (2008).
31. A. Reina *et al*., Transferring and identification of single- and few-layer graphene on arbitrary substrates. *J. Phys. Chem. C* **112**, 17741–17744 (2008).
32. Y. Han, K. X. Nguyen, Y. Ogawa, J. Park, D. A. Muller, Atomically thin graphene windows that enable high contrast electron microscopy without a specimen vacuum chamber. *Nano Lett.* **16**, 7427–7432 (2016).
33. Y. Han, *Uncovering Atomic Structures in Two-Dimensional Lateral Heterojunctions* (Cornell University, 2018).
34. A. Rohou, N. Grigorieff, CTFFIND4: Fast and accurate defocus estimation from electron micrographs. *J. Struct. Biol.* **192**, 216–221 (2015).
35. E. F. Pettersen *et al*., UCSF Chimera–A visualization system for exploratory research and analysis. *J. Comput. Chem.* **25**, 1605–1612 (2004).
36. T. D. Goddard *et al*., UCSF ChimeraX: Meeting modern challenges in visualization and analysis. *Protein Sci.* **27**, 14–25 (2018).
37. P. J. Artymiuk, P. M. Harrison, Data from "Solving the structure of human H ferritin by genetically engineering intermolecular crystal contacts." Protein Data Bank. https://www.rcsb.org/structure/1FHA. Deposited 20 December 1990.
38. X. Fan, J. Wang, J. L. Lei, H. w. Wang, Data from "Apo-state streptavidin." Protein Data Bank. https://www.rcsb.org/structure/6J6K. Deposited 15 January 2019.